9

Midlatitude Cloud Systems

GEORGE TSELIOUDIS AND KEVIN GRISE

In contrast to the tropics and subtropics, the middle latitudes are characterised by large meridional temperature gradients, created as a consequence of differential radiative heating between high and low latitudes. These meridional temperature gradients often concentrate in relatively narrow baroclinic zones that become unstable to wave-like perturbations called baroclinic eddies, or more commonly baroclinic storms or midlatitude cyclones. Baroclinic storms constitute the primary source of poleward energy transport at midlatitudes, which is accomplished through contrasting transports of warm air masses poleward (warm fronts) and cold air masses equatorward (cold fronts). Baroclinic storms also flux momentum into midlatitude regions, driving a region of enhanced westerly winds from the surface to the upper troposphere called the eddy-driven jet stream.

Baroclinic storms are the primary source of midlatitude cloud formation, and thus play an important role in determining the radiative and hydrologic budgets in midlatitude regions. High clouds of various vertical extents tend to form in the uplift regimes of the warm and cold fronts associated with the baroclinic storms, while low cloud decks often form in the subsidence regimes of the cold air masses that follow a cold frontal passage. As a result, the midlatitude cloud field encompasses almost the full range of cloud types, and the appearance of particular cloud types can be viewed as a tracer of midlatitude dynamic regimes. Because the clouds in the vicinity of the warm and cold fronts tend to be optically thick and often have tops in upper tropospheric layers, they produce substantial shortwave and longwave radiative signatures. Section **??** and Chapter 4 provide a detailed review of the shortwave and longwave radiative signatures of clouds. Briefly, the large optical depth of the clouds in the vicinity of the fronts promotes the reflection of incident solar radiation (a shortwave cooling effect), whereas the cold cloud top temperatures promote the reduction of outgoing longwave radiation to space (a longwave warming effect). In contrast, the low cloud decks in midlatitude cold air regimes have primarily a shortwave cooling effect, as their cloud-top temperature differs little from the underlying surface temperature.

These shortwave cooling and longwave warming effects make midlatitude clouds a key contributor to the global radiative budget and thus a potential source of significant radiative feedbacks in climate change situations (Chapter 13). Changes in the climate system, such as a climate warming, could affect meridional temperature gradients as well as the moisture availability of the atmosphere, which, through latent heat release, constitutes an additional energy source for baroclinic storms. Consequently, significant changes in the track and strength of baroclinic storms could occur with climate warming, and these changes would alter the midlatitude cloud field and produce radiative and hydrologic climate feedbacks. At the same time, altered cloud fields through their radiative effects and latent heat release have the ability to change temperature gradient patterns which in return can alter the characteristics of the midlatitude atmospheric circulation. The examination of midlatitude cloud processes and feedbacks, therefore, requires a detailed understanding of the relationships between the dynamical features of baroclinic storms and the properties of the clouds that they produce.

This chapter will examine in detail the relationships between cloud properties and atmospheric dynamics in midlatitude regions. Cloud structures and formation mechanisms in baroclinic storms will be examined first, with an emphasis on the latest satellite retrievals of cloud properties. Next, the climatologies of midlatitude clouds and their radiative properties will be discussed. Then the interactions of the midlatitude atmospheric circulation with clouds and their radiative properties will be examined, including an examination of the effects of clouds on the midlatitude circulation. Finally, the chapter will address how midlatitude clouds may be affected in a changing climate.

9.1 Midlatitude Cloud Structures

9.1.1 Cloud Structures in Baroclinic Storms

Baroclinic storm clouds have been extensively observed from both ground sites and space-based platforms, as they are integrally linked to weather forecasting at midlatitudes. Since the early days of weather observations, attempts have been made to explain the circulation features in a baroclinic storm and to map the cloud and precipitation structures that are formed in the different components of those circulation features. In this section, a brief description will be provided of early theories that explain the dynamical circulations and the resulting cloud formations in midlatitude storms, and then more recent results will be presented that use satellite retrievals, meteorological observations, and field campaign results to quantitatively characterise the properties of the

midlatitude cloud field and their relationship with midlatitude atmospheric dynamics.

9.1.1.1 Norwegian Cyclone Model

As early as the late 19th century, it was recognised that midlatitude baroclinic storms had a typical pattern in their cloudiness, such that systematic cloud observations might provide clues as to the development of weather systems. The first International Cloud Atlas published in 1896 allowed for the standardisation of remote cloud observations (Chapter 1). As a result of these early observations, the first conceptual model to depict the circulation and cloud features in a midlatitude cyclone, the Norwegian Cyclone Model, was formulated in the late 1910s and early 1920s by Jacob Bjerknes[1]. The model was constructed through the accumulation of surface observations of a multitude of storm passages, which typically include the appearance first of the warm frontal sector with southerly winds and warm temperatures followed by the passage of the cold front that turns the winds to northerly directions and drops the temperatures significantly. A schematic of the model is shown in Fig. 9.1, where the warm and cold air circulation regimes that form the warm and cold frontal regions around a Northern Hemisphere low pressure centre are shown with arrows, and the typical cloud and precipitation types that occur in each regime are drawn schematically and noted using cloud classification definitions. The classification of cloud types is based on the definitions used by surface weather observers that have changed very little over time (see Chapter 1). Those types identified by the weather observers as the primary clouds in midlatitude storms, included thin cirrus (Ci) and cirrostratus (CiStr) clouds occurring upstream of the storm centre, nimbus clouds (Ni) together with rain or snow along the warm and cold frontal zones, and altostratus clouds (AStr) in the cold air mass behind the cold front.

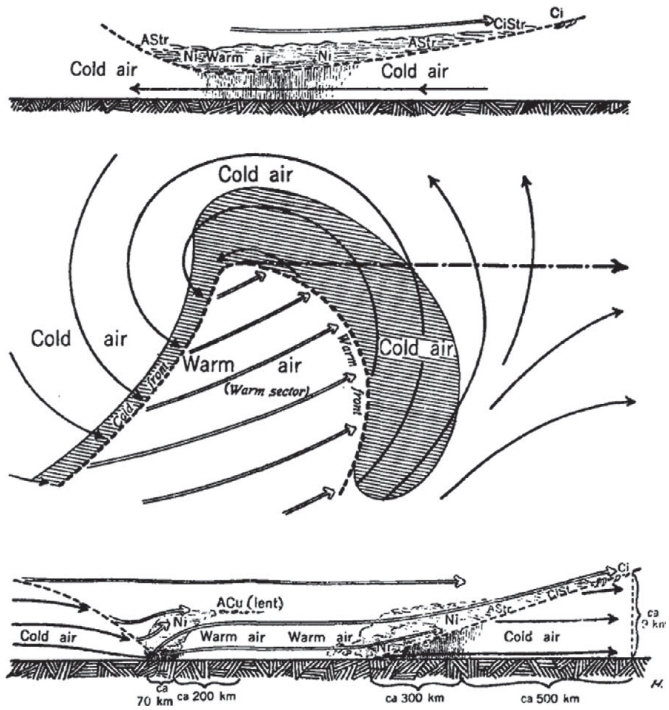

Figure 9.1 A schematic illustration of frontal clouds and precipitation constructed based on the Norwegian Cyclone Model, as conceptualised in the work of Bjerknes and Solberg (1922). The middle panel shows the warm and cold fronts and the movement of air around the storm centre, and the top and bottom plots show schematics of two west-east cross sections through the storm with indications of the locations of different cloud types, precipitation, and air movements. Adapted from Posselt et al. (2008). Copyright © 2008 American Meteorological Society (AMS).

9.1.1.2 Quasi-geostrophic theory

In the 1940s and 1950s, quasi-geostrophic theory was introduced, which helped to resolve with a high degree of accuracy the synoptic atmospheric motions associated with midlatitude baroclinic storms. A detailed explanation of quasi-geostrophic theory is provided in many atmospheric dynamics textbooks (see Further Reading at the end of the chapter). A brief summary is provided here.

The quasi-static (primitive) equations describe the dynamics of large-scale flows in the atmosphere. The origin of these equations is discussed in detail in Section **??** of Chapter 2. Using pressure as a vertical coordinate, the horizontal momentum equations can be written concisely as:

$$\mathrm{D}_t \boldsymbol{v}_p = -\boldsymbol{f} \times \boldsymbol{v} - \nabla_p \phi, \tag{9.1}$$

where ϕ is the geopotential and $\mathrm{D}_t = \partial_t + \boldsymbol{v}_p \cdot \nabla_p$. In midlatitude synoptic-scale weather systems, a scale analysis of the terms in Eq. (9.1) reveals an approximate balance between the Coriolis force and pressure gradient force terms, which is referred to as geostrophic balance:

$$0 \approx -\boldsymbol{f} \times \boldsymbol{v} - \nabla_p \phi. \tag{9.2}$$

Likewise, the horizontal wind that reflects an exact balance between the Coriolis and pressure gradient forces is referred to as the geostrophic wind $\boldsymbol{v_g}$:

$$\boldsymbol{v_g} = \{u_\mathrm{g}, v_\mathrm{g}, 0\} = (1/\boldsymbol{f}) \times \nabla_p \phi. \tag{9.3}$$

To first order, the winds in midlatitude weather systems are dominated by their geostrophic component. The ageostrophic component of the wind, $\boldsymbol{v_a} = \boldsymbol{v} - \boldsymbol{v_g}$, is comparatively much smaller, usually by an order of magnitude. Using this knowledge, the primitive equations can be greatly simplified by assuming that midlatitude synoptic-scale flows are approximately (but not exactly) in geostrophic balance ($\boldsymbol{v} \approx \boldsymbol{v_g} >> \boldsymbol{v_a}$). This *quasi-geostrophic approximation* simplifies the horizontal momentum equations (9.1) as follows:

$$\frac{\mathrm{d_g} \boldsymbol{v_g}}{\mathrm{d}t} = -f_0 \mathbf{k} \times \boldsymbol{v_a} - (\beta y) \mathbf{k} \times \boldsymbol{v_g}. \tag{9.4}$$

Here, note that, in the quasi-geostrophic approximation, the total derivative D_t in Eq. (9.1) is replaced by $\frac{\mathrm{d_g}}{\mathrm{d}t} = \frac{\partial}{\partial t}$

[1] **Jacob Aall Bonnevie Bjerknes** (1897–1975) was a Norwegian meteorologist, who is widely considered to be one of the pioneers of modern meteorology. His contributions range from his early work on the Norwegian cyclone model at the Geophysical Institute in Bergen, Norway to his later work on the general circulation and the El Niño-Southern Oscillation as a professor at the University of California at Los Angeles.

$+ u_\mathrm{g}\frac{\partial}{\partial x} + v_\mathrm{g}\frac{\partial}{\partial y}$. In other words, advection is approximated by the horizontal advection by the geostrophic wind; any vertical advection is neglected. Note also that the Coriolis parameter $\boldsymbol{f} = \{0, 0, f\}$ has been replaced by $\{0, 0, f_0 + \beta y\}$ using the so-called Beta-plane approximation where $f_0 >> \beta y$.

Similarly, using pressure as a vertical coordinate, the thermodynamic equation (**??**) can be written concisely as:

$$\mathrm{D}_t T + \frac{\omega}{c_p}\partial_p \phi = \frac{Q}{c_p}. \tag{9.5}$$

Here, we assume a dry atmosphere, such that the rhs of Eq. (9.5) equals the diabatic heating rate Q divided by the specific heat of dry air at constant pressure ($c_p = 1004\,\mathrm{J\,kg^{-1}\,K^{-1}}$).

We can rewrite the thermodynamic equation (9.5) in terms of the dry potential temperature θ (**??**):

$$\frac{\partial T}{\partial t} + u\frac{\partial T}{\partial x} + v\frac{\partial T}{\partial y} - S_p\omega = \frac{Q}{c_p}, \tag{9.6}$$

where $S_p = -\frac{T}{\theta}\frac{\partial \theta}{\partial p}$ is a measure of the static stability of the atmosphere in pressure coordinates. Under the quasi-geostrophic approximation, Eq. (9.6) simplifies to:

$$\frac{\mathrm{d_g}T}{\mathrm{d}t} - S_{p_0}\omega = \frac{Q}{c_p}, \tag{9.7}$$

where the subscript zero indicates a reference state temperature profile that varies only in the vertical direction ($S_{p_0} = -\frac{T_0}{\theta_0}\frac{\partial \theta_0}{\partial p}$).

It is often convenient to express the quasi-geostrophic horizontal momentum equations (9.4) in terms of the quasi-geostrophic relative vorticity $\zeta_\mathrm{g} = \frac{\partial v_\mathrm{g}}{\partial x} - \frac{\partial u_\mathrm{g}}{\partial y}$:

$$\frac{\mathrm{d_g}\zeta_\mathrm{g}}{\mathrm{d}t} = -f_0\left(\frac{\partial u_\mathrm{a}}{\partial x} + \frac{\partial v_\mathrm{a}}{\partial y}\right) - \beta v_\mathrm{g}. \tag{9.8}$$

Now, the quasi-geostrophic thermodynamic equation (9.7) and vorticity equation (9.8) can be combined to yield one diagnostic equation for vertical motions in midlatitude weather systems, the quasi-geostrophic omega equation (9.9):

$$\begin{aligned}\left(\nabla_p^2 + \frac{pf_0^2}{R_\mathrm{d}S_{p_0}}\frac{\partial^2}{\partial p^2}\right)\omega = &-\frac{1}{S_{p_0}}\nabla_p^2(-\boldsymbol{v_\mathrm{g}}\cdot\nabla_p T) \\ &- \frac{pf_0}{R_\mathrm{d}S_{p_0}}\frac{\partial}{\partial p}[-\boldsymbol{v_\mathrm{g}}\cdot\nabla_p(\zeta_\mathrm{g} + f)] - \frac{1}{S_{p_0}}\nabla_p^2\frac{Q}{c_p}.\end{aligned} \tag{9.9}$$

Assuming that the atmosphere is statically stable ($S_{p_0} > 0$), the term on the lhs of Eq. (9.9) behaves like the Laplacian of the vertical velocity (omega, ω). Recalling that the Laplacian operator can be approximated as a negative sign (particularly near minima or maxima in a scalar field), the lhs of Eq. (9.9) can be qualitatively interpreted as -ω, or rising motion. The first term on the rhs of Eq. (9.9) is related to the Laplacian of temperature advection by the geostrophic wind on constant pressure surfaces. This term implies that warm air advection is associated with -ω (rising motion) and cold air advection is associated with +ω (sinking motion). The second term on the rhs of Eq. (9.9) is related to the differential absolute vorticity ($\zeta_\mathrm{g} + f$) advection by the geostrophic wind on constant pressure surfaces. This term implies that cyclonic vorticity advection increasing with height (decreasing with pressure, $\frac{\partial}{\partial p}$) is associated with -$\omega$ (rising motion) and anticyclonic vorticity advection increasing with height is associated with +ω (sinking motion). Finally, the third term on the rhs of Eq. (9.9) is related to the diabatic heating rate, including effects from radiation and the latent heat of condensation. This term implies that diabatic heating is associated with -ω (rising motion) and diabatic cooling is associated with +ω (sinking motion). The diabatic heating term is often neglected, if air motions are assumed to be adiabatic.

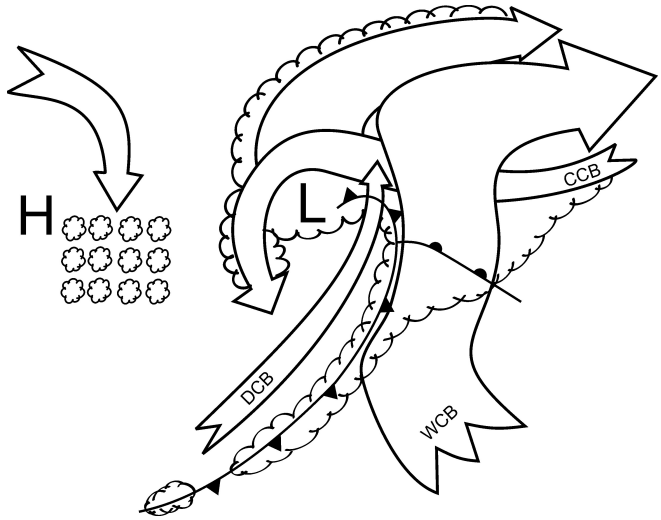

Figure 9.2 A schematic view of the conveyor belt model for the air circulation in midlatitude storm systems. The figure shows the positions of the fronts, the low-pressure centre (labeled as L), a high-pressure centre (labeled as H), and the three major conveyor belt circulations (warm conveyor belt: WCB, cold conveyor belt: CCB, and dry conveyor belt: DCB). The sense of circulation assumes $f > 0$ and would be reversed for $f < 0$, as in the Southern Hemisphere.

9.1.1.3 The "conveyor belt" model

Using knowledge from quasi-geostrophic theory, the Norwegian Cyclone Model can be extended into the so-called conveyor belt model, which is a full-scale model of the circulation, cloud, and precipitation components of baroclinic storms. The conveyor belt model is summarised in Fig. 9.2 and includes three major circulation features ("conveyor belts") surrounding the low-pressure centre of a baroclinic storm. Note that the latitudinal transports shown in Fig. 9.2 and discussed below apply to the Northern Hemisphere ($f > 0$) and must be reversed for Southern Hemisphere ($f < 0$) baroclinic storms.

The first feature of the conveyor belt model is a warm conveyor belt that originates at low levels in the southeastern quadrant of the storm and carries warm, moist air towards the north. This warm, moist air mass is often convectively unstable and therefore produces convective clouds and precipitating systems, including squall lines and strong thunderstorms. Even in the absence of convection, however, the large scale lifting of the warm, moist air by the approaching

cold front produces thick clouds with high tops that often precipitate. As the warm conveyor belt moves northward, this air motion is associated with warm air advection, and thus consistent with Eq. (9.9), the air rises as it flows northward and lifts over the warm front. This large-scale rising motion often produces large regions of stratiform cloud cover and precipitation ahead of the warm front. As the warm conveyor belt ascends, it is deflected to the east by the strong westerly winds in the midlatitude upper troposphere. As the warm conveyor belt moves to the east and northeast of the storm centre, the lifted moist air forms cirrostratus clouds that thin and change to cirrus as the air stream moves further eastward. Therefore, the appearance of cirrus clouds moving into a midlatitude region from the west is considered a harbinger of a storm passage.

The second circulation feature of the conveyor belt model is a cold conveyor belt that originates to the northeast of the low-pressure centre and brings cold air westward, as it passes underneath the warm conveyor belt and parallels the warm front along its northern edge. As the cold conveyor belt passes underneath the warm conveyor belt and warm frontal precipitation, it becomes significantly moistened and begins to rise slowly as it nears the low-pressure centre. The rising motion near the surface low is consistent with cyclonic vorticity advection increasing with height (from Eq. (9.9)), as an intensifying baroclinic weather system tilts westward with height such that the cyclonic vorticity advection associated with a mid-tropospheric trough (cyclonic vorticity anomaly) is typically positioned above the surface low. Once in the vicinity of the surface low, the cold conveyor belt splits into two branches: 1) an anticyclonic branch that is deflected eastward by the mid-tropospheric westerly winds and follows at lower levels the warm conveyor belt and 2) a cyclonic branch that wraps around the surface low, producing a distinctive comma-shaped cloud feature to the west of the surface low. Throughout its track, the low-level cold conveyor belt favours the formation of stratus cloud decks and fogs, which are often enhanced by evaporating precipitation falling from the warm conveyor belt above. Further to the west of the low-pressure centre, shallow cumulus cloud decks often form over ocean, as the cold air advection from the cyclonic circulation of air passes over warmer ocean waters.

The final circulation feature of the conveyor belt model is a dry conveyor belt. The dry conveyor belt originates in the upper troposphere and descends cyclonically to the south of the surface low, creating a dry tongue, or dry slot, at the western edge of the cold frontal circulation. The descending motion of the dry conveyor belt behind the cold front is consistent with the cold air advection occurring in this region (from Eq. (9.9)).

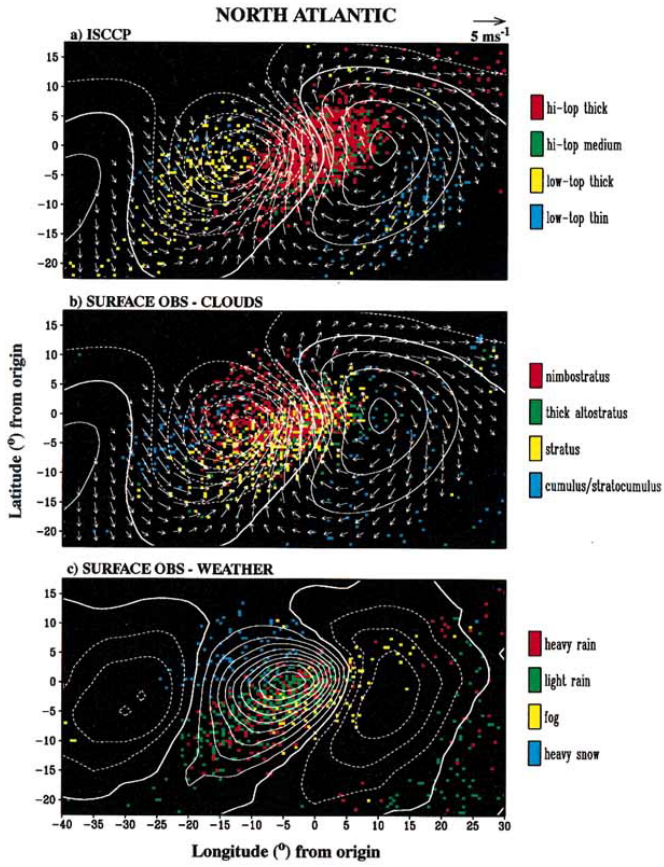

Figure 9.3 Patterns of the amount of selected cloud types based on (a) ISCCP data and (b) surface observations, and (c) frequency of occurrence of selected surface weather types, for a composite of midlatitude storms over the North Atlantic during the cool season (October–March). The colours on the plots indicate the relative abundance of a cloud type or weather regime as they are listed on the right of each plot, while the arrows (see scaling at top right) and contours (interval: 10 m) in (a) and (b) indicate the composite anomalous 1000 hPa wind and geopotential height fields from European Centre for Medium-Range Weather Forecasts (ECMWF) analyses, respectively. The composite anomaly pattern for the vertical velocity ω (with positive values indicating upward motion) from the ECMWF data is shown as contours (interval: $2 \times 10^{-2}\,\mathrm{Pa\,s^{-1}}$) in (c). Solid (dashed) contours indicate positive (negative) values. Adapted from Lau and Crane (1997).

9.1.1.4 Satellite retrievals of storm cloud properties

Surface weather observers provided these first, qualitative descriptions of the cloud structures in midlatitude baroclinic storms. Since the early 1980s, retrievals of cloud, radiation, and precipitation properties from satellite instruments have started to provide more quantitative information about the radiative and hydrologic structures of the global cloud field. Satellite retrievals provide detailed properties of midlatitude clouds and therefore make it possible to quantitatively relate those properties to the properties of the baroclinic storms that constitute the primary mechanism for the formation of these clouds.

A composite of satellite and surface retrievals of cloud and precipitation properties in a baroclinic storm is shown in Fig. 9.3. The satellite cloud property retrievals come from the International Satellite Cloud Climatology Project (ISCCP) while the cloud type and weather type observations come from surface weather observers (see Chapter 1 for a detailed discussion of cloud observing systems). The figure

shows a composite for cyclones over the North Atlantic, for the ISCCP cloud type retrievals (top), the surface observers' cloud types (middle), and the surface observers' weather types (bottom). The satellite definition of cloud height is based on a satellite measurement of the thermal emission from the top of the cloud, which indicates the temperature and therefore the vertical location of the cloud radiative top. The definition of cloud optical thickness is based on the cloud reflectance of solar radiation, which is indicative of the vertical thickness of the cloud and the density of the water and/or ice in it (Chapter 3). It is remarkable that the classical view of the cloud distribution around baroclinic storms derived first by surface observers as early as the late 19th century (Fig. 9.1) is verified with high accuracy by the global satellite retrievals and the more recent surface observer data; high-top thick and high-top medium or nimbostratus and altostratus clouds along with heavy precipitation dominate the warm and cold frontal regions of the storm, while low-top thick and low-top thin or stratus and cumulus/stratocumulus clouds along with snow are found in the cold air outbreak region behind the storm. One major difference between the surface observers and the satellite cloud types relates to the fact that the surface observers find large amounts of stratus cloud in the frontal sectors where the satellite retrieves higher top thick clouds. This is due to the bottom-up view of the surface observers versus the top-down view of the satellite and the fact that cloud top is not readily retrievable from the surface when the sky is fully covered by cloud.

The cloud structures derived by surface observers and by the first satellite cloud retrievals provide an illustration of the average structure of cloud type distribution in a typical midlatitude storm. However, cloud cover and cloud type distributions tend to vary widely both with changes in the strength of the baroclinic storms as well as with changes in atmospheric conditions that the storm is embedded in, such as the moisture availability of the atmosphere. In recent years, the global, multi-year nature of satellite observations along with reconstructions of atmospheric conditions by reanalysis datasets, allow us to analyse large ensembles of baroclinic storms and to derive meaningful classifications that make it possible to examine how the cloud structures and properties change with changing dynamic and thermodynamic conditions. Figure 9.4 illustrates the change in high clouds in midlatitude storms with changing storm strength (horizontal axis) and moisture availability of the atmospheric column (vertical axis). Here the strength of the storm is measured by the pressure value of the storm's low pressure centre. It can be seen that the amount of high cloud in a storm is strongly dependent on the storm strength since, for the same atmospheric moisture conditions, high clouds become more abundant and cover a larger region along the cold and warm frontal zones as the storm strength increases. The dependence of high cloud amount on atmospheric moisture availability is much weaker than the dependence on storm strength.

The first generation of satellite observations included cloud imagers that were able to retrieve cloud properties such as cloud top temperature and optical depth from radiances and irradiances originating from the cloud top. These measurements provided information on the column-mean cloud properties but did not provide information on the vertical variability of the cloud layers. The advent of active remote sensing measurements from space with the launch of the CloudSat radar and the CALIOP LIDAR in 2006 made it possible to examine the vertical distribution of cloud layers in the vicinity of baroclinic storms. Figure 9.5 shows a cross-section of the vertical profile of cloud layers in a baroclinic storm over the North Atlantic, derived from CloudSat radar retrievals. It can be seen that there is again a remarkable similarity of vertical structure with the cross-section of the cloud vertical profiles derived by the Norwegian cyclone model some 80 years earlier and shown in Fig. 9.1. The cloud type progression during the storm passage, with the cirrus and cirrostratus clouds ahead of the storm, the nimbostratus clouds along the frontal zones, and the low-top post-frontal clouds, is now verified through the use of radar retrievals. However, the use of active remote sensing also makes clear the existence of multi-layered clouds in the storm, a detail that cannot be readily resolved either from passive remote sensing or from surface observations. The pre-frontal cirrus are accompanied by low thin cloud decks, while part of the

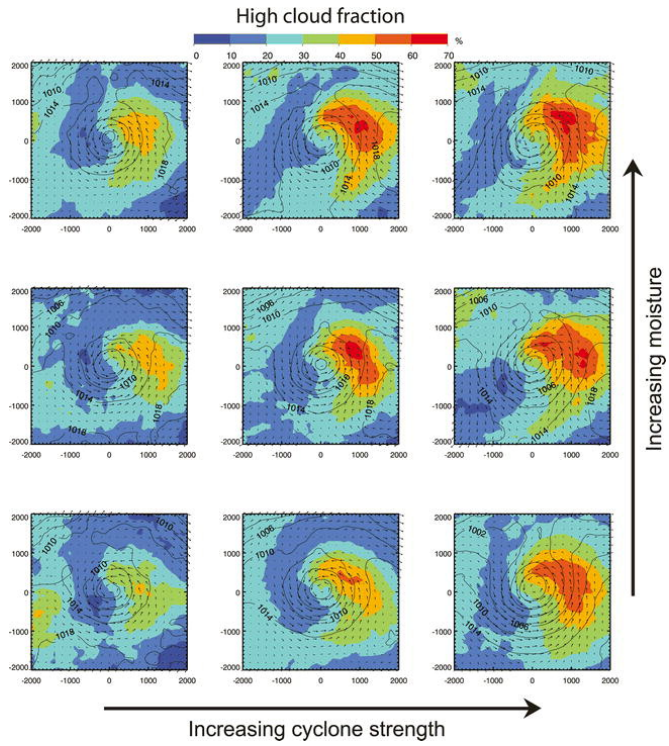

Figure 9.4 Composites of the amount of high cloud from midlatitude storms (cyclones) in all the major storm tracks, classified by the cyclone strength (increasing left to right) and the atmospheric moisture (increasing bottom to top). Cyclone strength is defined as the mean wind speed within 2000 km of the low-pressure centre and the atmospheric moisture as the mean water vapour path within 2000 km of the low-pressure centre. The composite mean surface pressure contours (in hPa) and surface wind vectors are also shown. Adapted from Field and Wood (2007). Copyright © 2007 American Meteorological Society (AMS).

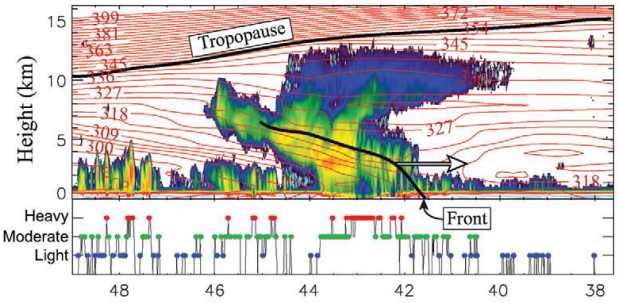

Figure 9.5 Cross-section along a North Atlantic baroclinic storm of CloudSat observed radar reflectivity (dBZ, colour shaded), overlaid with ECMWF-analysed equivalent potential temperature (K, solid red lines). The positions of the cold front and tropopause are marked with heavy black lines, and the direction of movement of the front is indicated with a white arrow. CloudSat-estimated precipitation rate is depicted directly below the plot of observed reflectivity. Adapted from Posselt et al. (2008). Copyright © 2008 American Meteorological Society (AMS).

cold frontal clouds are formed by two distinct thick layers of low and high cloud tops. This explains the difference in the view of the frontal clouds between satellite and surface observations shown in Fig. 9.3.

9.1.2 Regional patterns of midlatitude cloud organisation

The observational analyses presented so far show that, at synoptic scales, baroclinic storm systems constitute a major source of the variety of cloud types, and that cloud cover and type varies significantly depending on location within the baroclinic storm domain. High clouds dominate the warm conveyor belt circulation while low clouds occur in the cold conveyor belt. When averaged to form a climatology, however, the midlatitude cloud field does not show the pronounced regional patterns found in other climate regimes, other than some distinct cloud cover differences between land and ocean in the Northern Hemisphere. This relative uniformity of the midlatitude cloud field is due to the transient nature of baroclinic storms, which tend to distribute cloud amounts in a somewhat uniform manner throughout the three major oceanic storm tracks, located across the North Atlantic, North Pacific, and Southern Oceans.

The midlatitude storm tracks have been thoroughly documented and studied for well over a century, as they constitute the major weather makers for many of the world's populated regions. Midlatitude storms are commonly tracked by following the movement of the low-pressure centre that constitutes the centre of the storm over the duration of a storm's lifecycle (from cyclogenesis to cyclolysis). Storm tracking can either be performed manually (by hand) or through the use of an automated computer algorithm, which applies propagation and direction criteria to follow a low-pressure centre. Figure 9.6 shows two maps of the North Atlantic storm track, the top map coming from the climatology atlas

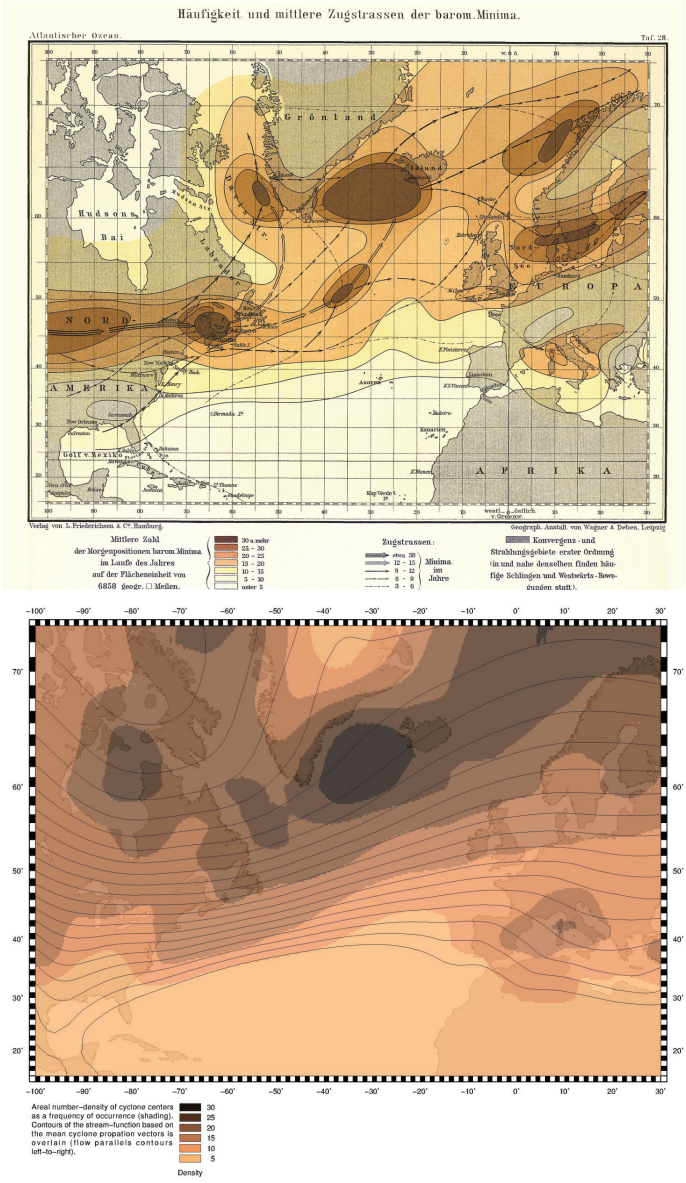

Figure 9.6 (Top) Frequency of surface lower pressure centres (colours) and density of centre paths (arrows) over the course of a year from the 1882 Köppen climatology atlas. (Bottom) Areal number density of cyclone centres (colours) and stream function of mean cyclone propagation from a 15-year climatology (2000–2015), derived using the storm tracking analysis of Bauer et al. (2016).

published by Wladimir Köppen[2] in 1882 and the bottom map coming from the application of a storm tracking algorithm on sea level pressure data over the years 2000–2015. It is remarkable to note the similarities between the two maps, given the sparse observational network available near the end of the 19th century. Several centres of large storm

[2] **Wladimir Köppen** (1846–1940) was a Russian-born climatologist, who spent much of his professional career at the German Naval Observatory in Hamburg. He is best known for establishing the Köppen classification of the world's climate zones, but was also an author on the first International Cloud Atlas (see Section **??**).

activity are present in both maps, including the maximum between Greenland and Iceland (the Icelandic Low) and the secondary storm track in the Mediterranean region. The location of the storm track is not necessarily stationary in time. There is some evidence that suggests that the North Atlantic storm track shifted poleward over the latter half of the 20th century. The potential effects of this storm track shift on the cloud field and its radiative effects are discussed in Section 9.3.1.

Some of the highest cloud amounts on the planet are observed in the midlatitude storm tracks (see Fig. **??** in Section **??**). In the three major oceanic storm tracks, annual mean total cloud cover is almost everywhere higher than 70%, and shows only weak regional patterns over the Northern Hemisphere oceans. In those basins, cloud cover tends to be higher in the western parts, maintaining values above 80% especially in the winter season when the storm tracks are generally most active. These larger cloud covers are caused by larger amounts of high-top clouds in the western basins, while low cloud amounts are somewhat higher in the eastern parts of the Northern Hemisphere ocean basins. The western parts of the basins are the cyclogenesis areas of the oceanic storm tracks (Hoskins and Hodges, 2002), and storms tend to produce larger amounts of high clouds in their formation stages than in their decay stages. Low cloud decks, on the other hand, occur more frequently in the eastern parts of the basins, because a) the subtropical and lower midlatitude parts of the Eastern North Atlantic are dominated by the semi-permanent Azores high pressure system, which tends to deflect storm tracks to the north (Fig. 9.6) and favours the formation of stable boundary layers and stratocumulus cloud decks, and b) in the eastern North Pacific, cold surface waters favour the formation of fogs and stratocumulus clouds through mechanisms explained in more detail in Chapter 8.

Midlatitude continental total cloud cover ranges in the annual mean between 40% and 70% and is, therefore, significantly lower than the midlatitude oceanic cloud cover. This is true for all cloud types with the exception of high thin cirrus clouds. The overall lower continental cloud covers are due both to the smaller moisture supply of the land compared to the ocean surface and to the overall weaker storm systems occurring over land. The continental storm tracks also tend to have smaller frequencies of storm systems than the oceanic storm tracks, partly because of shorter-lived storms over land. These factors contribute to the lower cloud cover over midlatitude continents.

The large amounts of midlatitude continental cirrus clouds are primarily orographic in nature. Orographic cloud formation occurs preferably on the leeward side of mountain ranges, as eastward flowing air is lifted by the mountains and cools forming cloud layers throughout the extent of the resulting gravity wave. Orographic cirrus coverage can reach values of about 30%, thus constituting a major contributor to the total cloud cover in regions downwind from major mountain ranges, such as the Rocky Mountains in North America, the Andes Mountains in South America, and the Himalayas in Asia.

9.2 Effects of midlatitude clouds on the atmospheric radiation budget

In the climatology, midlatitude clouds exert stronger effects on the Earth's top-of-atmosphere (TOA) radiative budget than clouds in any other latitude band. Annual mean shortwave cloud radiative cooling at TOA in the midlatitude regions ranges between 30–90 $\mathrm{W\,m^{-2}}$, and these values are some of the largest observed on the planet, comparable only to the values found in the tropical Western Pacific warm pool region, Intertropical Convergence Zone (ITCZ), and the stratocumulus regions of the eastern subtropical ocean basins (Fig. **??**). Midlatitude longwave cloud radiative warming ranges between 20–50 $\mathrm{W\,m^{-2}}$, lower only than the values observed in the ITCZ, the tropical Western Pacific, and the deep convective regions in the Amazon and equatorial Africa (Fig. **??**). As a result, net cloud radiative cooling in the midlatitudes ranges between 10–40 $\mathrm{W\,m^{-2}}$, only rivalled by the net cloud radiative cooling in the stratocumulus regimes in the eastern subtropical ocean basins (Figs. **??** and **??**). The large radiative cooling effect of midlatitude clouds makes them a significant contributor to the equator-to-pole temperature difference and hence acts to strengthen the large-scale atmospheric circulation (see Section 9.3.2).

As mentioned in the previous section, the transient nature of baroclinic storms distributes clouds, and therefore their radiative effects, rather uniformly along the major storm tracks. Large regional differences occur mainly between Northern Hemisphere land and ocean regions. Shortwave cloud radiative cooling over land ranges between 30–60 $\mathrm{W\,m^{-2}}$ while over ocean it ranges between 40–90 $\mathrm{W\,m^{-2}}$. Shortwave cooling maxima occur in the cyclogenesis regions in the western parts of Northern Hemisphere ocean basins, and relative minima in shortwave cooling occur in the cyclolysis regions in the eastern parts of the ocean basins (Fig. **??**). Cloud longwave warming over land ranges between 20–40 $\mathrm{W\,m^{-2}}$ with the maxima occurring in the cirrus prone regions downwind from the Andes, the Rockies, and the Himalayas. Cloud longwave warming over ocean ranges between 30–50 $\mathrm{W\,m^{-2}}$ with the maxima occurring in the high-cloud prone cyclogenesis regions (Fig. **??**). The values listed here are annual mean values. However, in the midlatitudes, cloud radiative effects vary significantly with season, both because of seasonal storm track variability and the significantly lower solar insolation during the winter season. The lower insolation during winter reduces the wintertime shortwave cloud radiative effect, as by definition, a cloud of a certain optical depth will reflect less solar radiation in the winter than in the summer.

It is important to note here that the two components of the cloud radiative effect, the shortwave cooling and the longwave warming, manifest themselves at different heights in the atmospheric column. Shortwave cooling manifests itself at the surface and, therefore, affects surface-atmosphere energy exchanges and temperature gradients in the boundary layer. The longwave warming, on the other hand, manifests itself in the atmospheric column with emphasis on the upper troposphere. As a result, longwave warming, along

with latent heat release, plays a significant role in the vertical distribution of energy exchanges and in determining temperature gradients in the upper troposphere. The customary addition of the shortwave and longwave cloud radiative effects to yield a net TOA cloud radiative effect does not properly resolve the different nature of the two contrasting effects, and is only useful in determining the net cloud contribution to the overall atmospheric energy budget. A net zero TOA cloud radiative effect that arises from the cancellation of contrasting shortwave and longwave cloud radiative effects implies vertical heating gradients that will be balanced by atmospheric circulation changes, which in turn can alter the cloud field and affect the radiative budget. Therefore, a net zero TOA cloud radiative effect does not necessarily correspond to a state of radiative equilibrium.

At the synoptic scale, large cloud radiative effect differences occur among the different circulation regimes of baroclinic storms. The existence of clouds with different cloud top heights and optical depths in the different storm sectors creates distinct radiative signatures. One way to understand these signatures is to separate the cloud radiative effects into instances when the sea level pressure (SLP) is higher and lower than the climatological value. This separation captures the climatological signatures of high and low pressure regimes, respectively. Combined analysis of recent satellite observations and weather data shows that the shortwave flux differences between high and low SLP regimes are significant and can vary with season: in the winter an excess shortwave cooling of 5–20 $\mathrm{W\,m^{-2}}$ occurs in the low SLP regime while in the summer this excess cooling increases to 20–50 $\mathrm{W\,m^{-2}}$, mostly due to the higher amounts of solar insolation (Tselioudis et al., 2000). This excess cooling manifests itself at the surface and would act to stabilise the surface horizontal temperature gradients in the storm, as it occurs primarily in the warm sector of the storm. The longwave differences between high and low SLP regimes are uniform across seasons and show an excess longwave warming of 5–35 $\mathrm{W\,m^{-2}}$ in the low SLP regime. This excess warming is manifested mostly as an additional warming of the atmospheric column and would act to increase the upper tropospheric temperature gradients of the storm, as it occurs again in the warm sector of the storm.

9.3 Interaction of clouds with the midlatitude circulation

The results presented in the previous sections show that, at synoptic scales, the amount and type of cloud produced in a storm, and therefore the cloud radiative effect, depend on the strength of the storm and the moisture availability of the atmosphere (Fig. 9.4). This implies that changes in the strength of the midlatitude circulation or the atmospheric moisture content will initiate changes in the properties of the midlatitude cloud field that have the potential to produce strong cloud radiative feedbacks. Clouds, on the other hand, can also alter the atmospheric thermal structure through their diabatic effects, which can then impact the strength of the midlatitude baroclinic circulation. Hence, changes in the atmospheric circulation can modify clouds, and changes in clouds can in return modify the atmospheric circulation.

For a discussion of the interaction of midlatitude clouds with the atmospheric circulation, it is crucial, therefore, to examine in brief the properties and processes of the midlatitude atmosphere that determine the strength and character of its circulation. From the theoretical perspective, if one considers a purely zonal jet stream with geostrophic wind speed U_g that only depends on height z, then a suitable measure of the baroclinicity of the flow is the Eady growth-rate maximum:

$$\sigma_\mathrm{BI} = 0.31 \frac{f}{N} \left| \frac{\mathrm{d}U_\mathrm{g}}{\mathrm{d}z} \right|, \tag{9.10}$$

where f is the Coriolis parameter, and N is the Brunt-Väisällä frequency, a measure of the atmospheric static stability (Eq. (**??**); Table **??**). The coefficient of 0.31 is derived from numerical calculations (Lindzen and Farrell, 1980).

Assuming hydrostatic balance (**??**), the geostrophic wind (9.3) varies with height according to the thermal wind relationship:

$$\frac{\partial \boldsymbol{v_\mathrm{g}}}{\partial z} = \frac{g}{\boldsymbol{f}} \times \nabla(\ln T). \tag{9.11}$$

Substituting for $\frac{\mathrm{d}U_\mathrm{g}}{\mathrm{d}z}$ from Eq. (9.11), the maximum Eady growth rate can be written in terms of the magnitude of the meridional temperature gradient $\frac{\partial T}{\partial y}$:

$$\sigma_\mathrm{BI} = 0.31 \frac{g}{TN} \left| \frac{\partial T}{\partial y} \right|. \tag{9.12}$$

Eq. (9.12) implies that baroclinic storm generation depends on the existence and magnitude of meridional temperature differences and the static stability of the midlatitude atmosphere. According to Eq. (9.12), any processes that enhance the static stability of the midlatitude atmosphere would act to suppress baroclinic storm generation, whereas any processes that enhance the meridional temperature gradient would act to promote baroclinic storm generation. This theoretical framework will be used as the basis for understanding the interactions between clouds and the midlatitude circulation discussed in this section. Results from recent studies of both observations and model simulations will be examined.

9.3.1 Influence of the midlatitude circulation on cloud properties

Baroclinic storms propagate preferentially within the midlatitude storm track regions of the North Atlantic, North Pacific, and Southern Oceans, so at planetary scales, midlatitude cloud and radiation changes can result either from a) changes in the location of those storm track regions or b) from changes in the strength or frequency of the individual baroclinic storms.

9.3.1.1 Changes in storm track position

The positions of the baroclinic storm tracks at both Northern and Southern Hemisphere midlatitudes are not static in

time, but rather fluctuate between more poleward and more equatorward positions on the timescale of approximately 10 days. These modes of unforced variability in the extratropical atmospheric flow are referred to as the Northern and Southern Annular Modes, respectively. The exact dynamics that govern the annular modes are still being researched. In brief, from Eq. (9.12), the maximum growth rates of baroclinic eddies occur where the meridional temperature gradients are largest. The baroclinic eddies formed at the latitude of the maximum meridional temperature gradient act to flux momentum back toward their formation region, driving a region of enhanced westerly winds from the surface to the upper troposphere called the eddy-driven jet stream. Consequently, if the location of the strongest meridional temperature gradient is perturbed poleward or equatorward, the baroclinic storm tracks and eddy-driven jet stream will closely follow. The momentum fluxes by the baroclinic waves are thought to be crucial in maintaining the storm track and eddy-driven jet stream in a more poleward or equatorward position for 1–2 weeks (Lorenz and Hartmann, 2001).

The latitudinal shifts in the baroclinic storm tracks and eddy-driven jet stream associated with the annular modes should be accompanied by corresponding cloud property shifts, particularly in the high cloud field, as the intense upward motions in individual baroclinic storms should closely follow the location of the storm tracks and jet stream. In addition, the cloud shifts should be associated with coherent changes in the cloud radiative effects. Poleward storm track shifts are also sometimes linked to increases in midlatitude storm strength, but this may be due to the lower climatological sea level pressure closer to the poles which makes a storm shift appear as an increase in the SLP-defined storm strength even if the storm circulation is not stronger.

Analyses of both observational data gathered over the last 35 years and of model simulations can be used to examine the relationships between eddy-driven jet shifts and cloud properties. High clouds, for the most part, tend to shift consistently with the eddy-driven jets in most ocean basins and seasons. The high cloud shifts produce distinct longwave atmospheric warming in the region of increased high cloud cover (i.e., the latitudes toward which the jet and storm tracks have moved) and cooling in the region of reduced high cloud cover (i.e., the latitudes from which the jet and storm tracks have moved). Changes in the shortwave cloud radiative effects with eddy-driven jet shifts, however, are more complicated because low-top clouds do not respond in a systematic manner to eddy-driven jet shifts. The response of low-top clouds to eddy-driven jet shifts varies widely by ocean basin and often differs between observational data and model simulations (Grise and Medeiros, 2016).

In the North Atlantic, the poleward movement of the eddy-driven jet stream during the winter season produces a shortwave warming effect in areas equatorward of the jet, caused by a reduction in the total cloud amount in those areas that allows more sunlight to reach the ocean surface. The North Atlantic high cloud and cloud radiative effect changes are illustrated in Fig. 9.7, which shows the changes in high cloud amount (top panel), longwave cloud radiative effect (middle panel) and shortwave cloud radiative effect

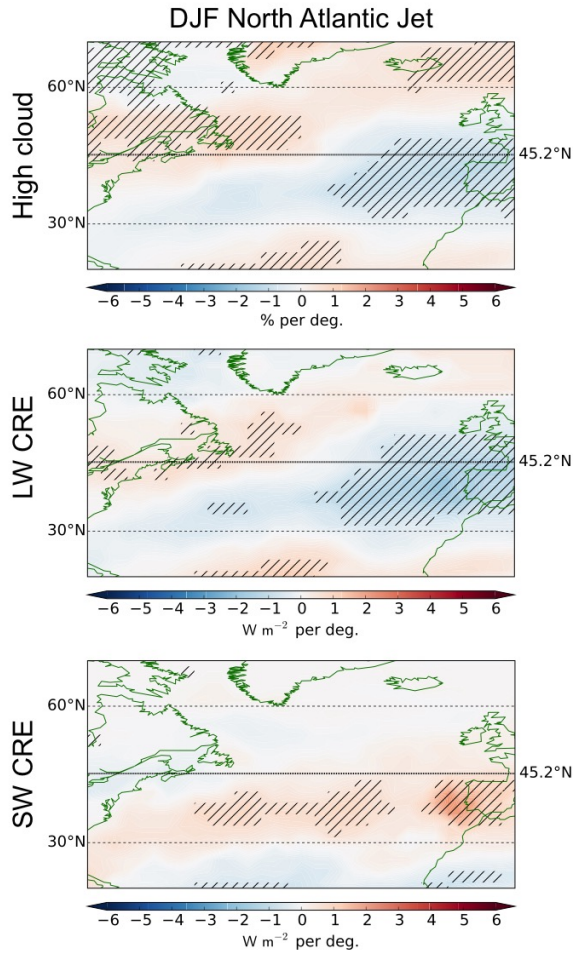

Figure 9.7 Changes in high cloud amount (top panel), longwave cloud radiative effect (LW CRE) (middle panel) and shortwave cloud radiative effect (SW CRE) (bottom panel) for a one-degree poleward shift of the eddy-driven jet during winter over the North Atlantic ocean. The high cloud changes are shown in percentage units and the radiation changes in $\mathrm{W\,m^{-2}}$. Shaded regions denote statistically significant changes and the thicker horizontal line shows the mean position of the eddy-driven jet for that region and season. Adapted from Tselioudis et al. (2016).

(bottom panel) for a one-degree poleward shift in the North Atlantic jet during winter. The high cloud amount shows a dipole change, with increases of 1–2% in the northern part of the basin and decreases of similar magnitude in the southern part of the basin, while the longwave cloud radiative effect change shows a corresponding warming of 1–2 $\mathrm{W\,m^{-2}}$ in the northern part of the basin and a cooling of 1–3 $\mathrm{W\,m^{-2}}$ in the southern part of the basin. The shortwave cloud radiative effect change shows mainly a 1–3 $\mathrm{W\,m^{-2}}$ warming in the southern part of the basin, since in the northern part of the basin, solar insolation is very small during the winter and therefore cloud changes do not produce a significant shortwave radiative signature.

In contrast to the North Atlantic winter season, in the summertime Northern Hemisphere and in all seasons in the

Southern Hemisphere, a poleward eddy-driven jet shift produces a small shortwave cloud radiative cooling anomaly at the poleward part of the midlatitude domain (∼50° to 60° latitude) and does not produce any observable shortwave cloud radiative warming anomaly equatorward of the jet position. Understanding these complicated signatures is an area of active research, as they are not represented well in many present-day global climate models. The shortwave cooling at higher latitudes is likely produced through an increase in the liquid water path of the storm cloud field. The lack of shortwave warming equatorward of the jet shift is likely due to the presence of large amounts of low-top clouds in the lower midlatitude areas (∼30° to 45° latitude) of these ocean basins, and these clouds do not appear to respond in a coherent manner to eddy-driven jet shifts. As a matter of fact, a poleward movement of the eddy-driven jet is often correlated with a poleward expansion of the subsiding branch of the Hadley circulation, which creates favourable conditions for the formation of more extensive low cloud decks at the equatorward side of the midlatitude zones. Such increases in low clouds would negate the radiative effects of any decreases in the high cloud field with the poleward storm track shift. Consequently, variability of the midlatitude circulation and its effect on the midlatitude cloud field cannot be examined in isolation from the variability of the large-scale tropical circulation.

9.3.1.2 Changes in strength and frequency of baroclinic storms

Changes in midlatitude clouds and their radiative properties are also expected with changes in the strength and frequency of individual baroclinic storms. From Eq. (9.12), recall that the growth rates of baroclinic storms are closely related to the strength of the meridional temperature gradient and to the atmospheric stability, with more unstable lapse rates promoting greater baroclinic eddy growth. As illustrated in Fig. 9.4, the amount of high cloud in baroclinic storms depends strongly on storm strength changes and, to a lesser extent, on the moisture availability of the atmospheric column. Table 9.1 quantifies the changes in cloud radiative effect associated with changes in midlatitude storm strength and frequency, as derived from observations. The values in Table 9.1 represent the shortwave and longwave cloud radiative effect responses to a 7% decrease in the overall midlatitude storm frequency and to a 5% increase in overall storm intensity. These changes in frequency and intensity were used because they represent typical values occurring in climate warming simulations (see Section 9.4 for further discussion of climate change impacts on midlatitude clouds).

The results in Table 9.1 show that changes in storm strength and frequency have opposite effects on cloud radiative effects. Storm strength increases produce shortwave cooling and longwave warming through the production of optically thicker clouds with higher cloud tops. These cloud changes occur in the cold and warm frontal sections of the storms as shown in Fig. 9.4. The shortwave cooling is of order 2–5 $\mathrm{W\,m^{-2}}$, depending on hemisphere and season, and the longwave warming is of order 1.5–2.5 $\mathrm{W\,m^{-2}}$. As a result, a 5% increase in storm strength results in a net cooling of order 1.5 $\mathrm{W\,m^{-2}}$. It must be noted again, however, that shortwave cooling materialises at Earth's surface while longwave warming materialises in the tropospheric column, and therefore the shortwave and longwave effects affect fundamentally different processes in the Earth system.

Storm frequency decreases, on the other hand, produce shortwave warming and longwave cooling through an overall decrease in the amount, optical depth, and height of the cloud field. The shortwave warming is of order 1.5–2.5 $\mathrm{W\,m^{-2}}$ and the longwave cooling is of order 0.5–1.5 $\mathrm{W\,m^{-2}}$. As a result, a 7% decrease in storm frequency results in a net warming of order 1 $\mathrm{W\,m^{-2}}$. It is clear that the net cloud radiative effect of any combined storm strength and frequency change depends on the relative magnitude of change of the two dynamic components and the hemisphere and season where they occur. For this particular storm change configuration, the overall radiative change is dominated by the shortwave cooling caused by the storm strength increase. Note that the magnitudes of the radiative signatures from these relatively modest changes in storm strength and frequency are of order 1–5 $\mathrm{W\,m^{-2}}$, implying the potential for strong radiative effects from climate perturbations in the characteristics of baroclinic storms.

9.3.2 Influence of clouds on the midlatitude circulation

Unlike the tropics where diabatic processes are the key driver of the atmospheric circulation, the midlatitude circulation is governed more strongly by the presence of large horizontal temperature gradients. As discussed above, the location and strength of the eddy-driven jet streams and storm tracks depend on the thermal structure of the midlatitude atmosphere, and midlatitude clouds apply thermal forcings to the atmospheric column, both through radiative and latent heating effects. Differential thermal forcing by the clouds can produce horizontal and vertical temperature gradients that in turn could influence the midlatitude circulation, including the eddy-driven westerly jets. This forcing can happen at different spatial scales ranging from the global and climate scales to the local and synoptic scales. The Eady growth rate equation (9.12) indicates that storm growth responds to both temperature gradients and static stability changes, and both of those processes can be induced by changes in the structure and the properties of the midlatitude cloud field.

Clouds produce atmospheric thermal gradients either through the release of latent heat via condensation or through their interactions with atmospheric radiation. At the synoptic scale, emphasis has been put on the release of latent heat because the cloud-induced radiative heating is generally smaller by an order of magnitude than latent heating, and because observations of cloud-modified radiative fluxes have been sparse and less reliable. At such synoptic and local scales, cloud diabatic effects can damp or amplify the in-atmosphere energy balance of atmospheric eddies depending on whether the passage of storm clouds tends to warm an otherwise warm atmosphere or to warm

		Winter		Summer	
		SW	LW	SW	LW
Northern Hemisphere	Increasing storm strength	-3.7	+1.5	-1.9	+1.6
	Decreasing storm frequency	+2.6	-1.4	+1.9	-1.0
	Net change	-1.1	+0.1	0.0	+0.6
Southern Hemisphere	Increasing storm strength	-4.9	+2.5	-3.7	+1.4
	Decreasing storm frequency	+1.4	-0.3	+1.9	-0.4
	Net change	-3.5	+2.2	-1.8	+1.0

Table 9.1. *Net TOA shortwave (SW) and longwave (LW) flux changes in* $\mathrm{W\,m^{-2}}$ *with storm strength and frequency over midlatitude bands (*$30^\circ N$–$65^\circ N$ *and* $30^\circ S$–$65^\circ S$*) for winter and summer seasons. Adapted from Tselioudis and Rossow (2006).*

an otherwise cold atmosphere. The cloud diabatic effects often depend on latitude and season as well as on the vertical distribution of the diabatic heating.

Modelling and observational studies generally show that latent heat release leads to stronger storms and faster storm development. In the vertically tilted structure of a baroclinic storm, the latent heat release associated with cloudy air ascending the frontal structure of the warm conveyor belt is often accompanied by evaporative cooling from precipitation falling into the dry air intrusion behind the cold front (Fig. 9.2). This creates a heating dipole along the front that increases baroclinicity, which could strengthen the storm circulation. Despite their relatively smaller magnitude, radiative heating terms could also play a role in affecting baroclinic storm development. As discussed in Section 9.2, shortwave cloud radiative cooling effects tend to dampen the surface horizontal temperature gradients in low pressure systems, while longwave cloud warming effects tend to strengthen the upper tropospheric horizontal temperature gradients. In addition, longwave cooling that peaks above the cloud top combined with longwave warming below can create vertical diabatic heating gradients especially near the tropopause, which can induce circulations that strengthen the amplitude of the baroclinic storm. It is difficult to observe diabatic heating rates with sufficient spatial and temporal resolutions to resolve interactions between clouds and synoptic-scale dynamics. However, modelling analyses indicate that latent heat release is an important contributor to the storm energy budget at the early stages of high latitude winter storms (Booth et al., 2013), while radiative effects could play an important role in the development of high latitude summertime storms when shortwave effects are the strongest. It is fair to say that we are still at the beginning stages of understanding the interactions between cloud-scale thermodynamic processes and synoptic-scale midlatitude weather systems.

On global climate scales, the radiative effects of midlatitude clouds, particularly the effects on shortwave radiation, are generally considered to be the most important diabatic cloud effects on the midlatitude circulation. Shortwave cloud radiative effects cool the surface and therefore modulate horizontal temperature gradients and surface baroclinicity, particularly during the summer season when the solar insolation at midlatitudes is maximised. The existence of bands of strong shortwave cloud radiative forcing over the midlatitude storm tracks introduces an additional cooling component that sharpens the meridional temperature gradient on the equatorward side of the midlatitude storm tracks, which affects the baroclinicity (see Eq. (9.12)) and could therefore subsequently feed back upon the strength and location of the eddy-driven jets and storm tracks. The strength of this shortwave cloud radiative forcing depends on the cloud amount and the optical depth of the midlatitude cloud field. It is important to also note, however, that the existence of shortwave cloud radiative cooling at middle latitudes decreases meridional temperature gradients on the poleward side of midlatitude ocean basins and therefore can decrease the baroclinicity in higher latitude regions. Therefore, the shortwave radiative effects of midlatitude clouds depend strongly on the mean position of the storm tracks.

Studies of the radiative effects of midlatitude clouds on the large-scale midlatitude circulation are done mostly in the context of atmospheric models, often run in idealised frameworks such as the aqua-planet framework in which the Earth's surface is entirely ocean. Such modelling studies suggest that cloud changes that favour increases in the gradient of absorbed shortwave radiation between high and low latitudes increase midlatitude baroclinicity and produce a poleward shift and a strengthening of the eddy-driven jet streams (Ceppi and Hartmann, 2016). Model simulations also suggest that cloud radiative effects within the atmosphere, achieved mostly through longwave absorption in the atmospheric column, exhibit important influences on the large-scale circulation. Model sensitivity experiments demonstrate that these in-atmosphere radiative effects strengthen the eddy-driven jet stream and increase eddy kinetic energy by as much as 30% (Li et al., 2015). This effect is achieved through an increase of the in-atmosphere meridional temperature gradient and decreases in static stability in the midlatitude upper troposphere.

The modelling results point to a strong dependence of the midlatitude circulation on cloud radiative effects. It must be noted, however, that atmospheric models include in their simulations strong biases in their midlatitude radiative budgets, manifested in most models through a strong positive bias in absorbed shortwave radiation at middle and high latitudes (Trenberth and Fasullo, 2010). This is due to the fact that most climate models simulate a midlatitude cloud field that includes too few yet too optically thick clouds. Models simulate high, optically thick cloud decks along the

warm conveyor belt circulations of midlatitude storms. However, for the most part, they fail to simulate the extensive middle and low cloud decks that occur in the cold air outbreak regimes that follow the passage of the frontal structures (Bodas-Salcedo et al., 2014). These cold air outbreak regimes are associated with large-scale subsidence, so the failure of models to accurately simulate low cloud decks here is consistent with their similar struggles in the subsiding regimes of the tropics and subtropics (Chapter 8). As a result, most climate models allow excess amounts of shortwave radiation to reach the midlatitude surface and at the same time misrepresent the horizontal radiative gradients that exist between the different sectors of baroclinic storms, which are important factors in the storms' development. The existence of these cloud errors and radiative biases make the results of model studies of midlatitude cloud/dynamics interactions difficult to interpret and motivates the need for stricter observational constraints.

9.4 Midlatitude clouds in a changing climate

The midlatitude cloud systems discussed in this chapter are likely to be significantly altered over the coming century (see also Chapter 13). With increasing greenhouse gas concentrations, the troposphere is expected to warm and the stratosphere is expected to cool, which will raise the height of the global tropopause. A rising tropopause height will allow high-topped clouds to extend to higher altitudes at midlatitudes, increasing their longwave radiative warming capacity. However, because many midlatitude clouds are composed in part of ice, a warming troposphere will also promote the existence of more in-cloud liquid, increasing the optical depth of these clouds and consequently their shortwave radiative cooling capacity. Furthermore, as the troposphere warms, the saturation vapour pressure will increase exponentially with temperature via the Clausius-Clapeyron relationship (Eq. (**??**); Fig. **??**), and thus there will be increased moisture availability for midlatitude clouds and the energetics of midlatitude storms. Absolute humidity gradients are also projected to increase, which would make mixing more effective in stabilising saturated regions.

The changing climate will also likely alter midlatitude circulation patterns. Global climate models suggest that, with increasing greenhouse gas concentrations, the storm tracks and eddy-driven jet streams will shift poleward, particularly in the Southern Hemisphere. The mechanisms for these poleward jet and storm track shifts are not well understood. Several leading hypotheses rely on the fact that, in a warming climate, upper tropospheric temperatures will increase substantially more than surface temperatures, particularly in the tropics and subtropics. The large warming of the tropical upper troposphere (compared to that at the surface) is due to the fact that the tropical atmospheric lapse rate is approximately moist adiabatic. Greater warming in the subtropical and midlatitude upper troposphere would enhance the static stability on the equatorward side of the present-day storm track, acting to suppress baroclinic eddy growth there (see Eq. (9.12)) and thus promoting a poleward shift of the storm track (Vallis et al., 2015). Because warming of the tropical upper troposphere strengthens the meridional temperature gradient in the upper troposphere-lower stratosphere, the enhanced meridional temperature gradient in the upper troposphere-lower stratosphere might also be a critical component in driving the poleward shift in the storm track and eddy-driven jet. A complicating factor is that, as the climate warms, enhanced warming of the Arctic surface due to ice-albedo feedbacks ("polar amplification") will act to reduce the surface pole-to-equator temperature gradient in the Northern Hemisphere, which has been shown to promote an equatorward shift in the storm tracks and eddy-driven jet stream in model experiments (Butler et al., 2010).

Regardless of the mechanism involved, systematic poleward jet and storm track shifts are likely to have fundamental impacts on midlatitude cloud fields (as noted in Section 9.3.1.1). Some recent satellite observations suggest that midlatitude cloud fields have already begun to shift poleward (Bender et al., 2012). Recent observed poleward jet and storm track shifts are more pronounced in the Southern Hemisphere and can be attributed, at least in part, to the existence of the Antarctic ozone hole, which is thought to have contributed to a pronounced poleward jet and storm track shift in the Southern Hemisphere summer months since the early 1980s. The ozone hole is associated with substantial cooling in the Southern Hemisphere polar lower stratosphere during spring and summer months, which enhances the meridional temperature gradient in the upper troposphere-lower stratosphere. Antarctic polar stratospheric ozone levels are expected to recover by the mid to late 21st century, so the Southern Hemisphere summertime storm tracks would be expected to return to a more equatorward position by the mid-21st century in the absence of increasing greenhouse gases.

The strength and frequency of individual midlatitude storms is also likely to be impacted by the changing climate. Enhanced warming in the upper troposphere compared to that at the surface would increase midlatitude static stability, which would have a weakening effect on storm intensity via Eq. (9.12). Likewise, enhanced warming of the Arctic surface would act to reduce the surface pole-to-equator temperature gradient in the Northern Hemisphere, reducing the surface baroclinicity available for the growth of baroclinic storms. However, the predicted increase in atmospheric moisture content and the upper tropospheric-lower stratospheric temperature gradient might be expected to increase the strength of baroclinic storms. There is little consensus about whether baroclinic storms will increase or decrease in strength in a warming climate, while there is some agreement among climate models that baroclinic storms will reduce in frequency, particularly in the Northern Hemisphere (Chang et al., 2012). As noted in the introduction to this chapter, the purpose of baroclinic storms is to transport energy from equator to pole. If the equator-to-pole temperature gradient is reduced, the amount of required energy transport would be reduced. Similarly, if the amount of moisture in baroclinic storms increases, weaker storms could attain the same required energy transport. From these sim-

ple arguments, fewer or weaker storms might be expected in a warmer climate. Systematic changes in storm magnitude and frequency will have fundamental impacts on midlatitude cloud fields and their radiative impacts, as noted in Section 9.3.1.2.

Midlatitude cloud changes induced directly by warming temperatures or indirectly through midlatitude circulation changes can potentially feed back on the position and strength of the atmospheric circulation via changes in horizontal and vertical temperature gradients in diabatic heating (as discussed in Section 9.3.2). It remains an area of active research as to how much midlatitude clouds and their responses to a changing climate will impact future changes in baroclinic storms and the large-scale midlatitude circulation.

Exercises

1. Using $\boldsymbol{v_g} = (1/\boldsymbol{f_0}) \times \nabla_p \phi$, show that the rhs of Eq. (9.1) is equivalent to the rhs of Eq. (9.4). Make the quasi-geostrophic Beta plane approximation.

2. Show that the thermodynamic equation for a dry atmosphere (9.5) can be rewritten in terms of the dry potential temperature θ (**??**) as Eq. (9.6).

3. Show that the quasi-geostrophic vorticity equation (9.8) can be derived from the quasi-geostrophic horizontal momentum equations (9.4).

4. Show that the quasi-geostrophic omega equation (9.9) can be derived from the quasi-geostrophic thermodynamic equation (9.7) and vorticity equation (9.8).

5. Explain why the Laplacian operator can be approximated as a negative sign in the interpretation of the quasi-geostrophic omega equation (9.9).

6. Using your knowledge of the quasi-geostrophic omega equation (9.9), draw a sketch of a typical midlatitude cyclone (as in Figs. 9.1 and 9.2). Label where the thermal advection, differential vorticity advection, and diabatic heating terms are likely to contribute to upward or downward motion.

7. The average daily solar insolation reaching the top of Earth's atmosphere is given by the following formula (see Hartmann (2016) for details):

$$\frac{S_0}{\pi}\left(\frac{\bar{d}}{d}\right)^2 [h_0 \sin\phi \sin\delta + \cos\phi \cos\delta \sin h_0], \qquad (9.13)$$

where $S_0 = 1360\,\mathrm{W\,m^{-2}}$ is the solar constant at Earth, $\bar{d} = 1.496 \times 10^{11}\,\mathrm{m} = 1$ AU is the mean earth-sun distance, d is the earth-sun distance, ϕ is latitude, and δ is the solar declination angle (the latitude at which the sun is directly overhead at noon, which varies from -23.45° to 23.45°). h_0 is the hour angle at sunrise and sunset (in radians), which is defined by $\cos h_0 = -\tan\phi \tan\delta$.

Using this formula, estimate the variation in solar insolation between the summer and winter solstices at 45°N and 45°S. The earth-sun distance on December 21 is 0.98376 AU, and the earth-sun distance on June 20 is 1.01618 AU.

8. Assuming a hydrostatic atmosphere (**??**), derive the thermal wind relationship (9.11) from the definition of the geostrophic wind (9.3). *Hint: You can assume that* $\boldsymbol{v_g}\frac{\mathrm{d}(\ln T)}{\mathrm{d}z}$ *is small and can be neglected.*

9. Using reanalysis data, plot the annual-mean climatology of the maximum Eady growth rate in the latitude-height plane. Explain the observed features within the context of the climatologies of the meridional temperature gradient and static stability.

10. Speculate on how increasing high and low cloud cover at midlatitudes may affect the midlatitude circulation. Justify your answer using the thermal wind equation (9.11) and the Eady growth rate equation (9.12).

Further Reading

This chapter provided an overview of a wide range of extratropical cloud issues, related to their properties, their formation mechanisms, and their interaction with radiation and with atmospheric dynamics. Each of those issues is examined in more detail in the resources listed below.

Section 9.1: Midlatitude Cloud Structures

Carlson, *Mid-Latitude Weather Systems* (Carlson, 1998) This book provides a detailed discussion of the observed structures and dynamics in extratropical cyclones from a synoptic meteorology perspective. Topics covered include the Norwegian cyclone model, baroclinic storm development, and quasi-geostrophic theory.

Cotton and Anthes, *Storm and Cloud Dynamics* (Cotton and Anthes, 1989) This book provides extensive coverage of the relationships between cloud formations and dynamical circulations across a range of mesoscale and synoptic-scale weather systems. Their Chapter 11 includes further detail on the relationships between clouds and dynamics in extratropical cyclones.

Holton and Hakim, *An Introduction to Dynamic Meteorology* (Holton and Hakim, 2013) This book provides a detailed introduction to atmospheric dynamics, ranging from fundamental concepts such as geostrophic and thermal wind balance to more advanced topics on the atmospheric general circulation. Their Chapters 6 and 7 provide further detail on quasi-geostrophic theory and baroclinic instability, respectively.

Section 9.3: Interaction of clouds with the midlatitude circulation

Ceppi and Hartmann, *Connections between clouds, radiation, and midlatitude dynamics: A review* (Ceppi and Hartmann, 2015) This short review article provides an overview of the recent scientific literature linking variability in midlatitude dynamics with clouds and their associated radiative feedbacks.

Section 9.4: Midlatitude clouds in a changing climate

Shaw et al., *Storm track processes and the opposing influences of climate change* (Shaw et al., 2016) This review article provides a detailed summary of the recent scientific literature on the dynamics of baroclinic storm tracks, their linkages with moist processes, and processes relevant for explaining their changes in a warming climate.

REFERENCES

Bauer, M. P., Tselioudis, G., and Rossow, W. B. 2016. A new climatology for investigating storm influences in and on the extratropics. *J. Appl. Meteorol. Climatol.*, **55**, 1287–1303.

Bender, F. A-M., Ramanathan, V., and Tselioudis, G. 2012. Changes in extratropical storm track cloudiness 1983–2008: Observational support for a poleward shift. *Climate Dyn.*, **38**, 2037–2053.

Bjerknes, J., and Solberg, H. 1922. Life cycle of cyclones and the polar front theory of atmospheric circulation. *Geophysisks Publikationer*, **3**, 3–18.

Bodas-Salcedo, A., Williams, K. D., Ringer, M. A., Beau, I., Cole, J. N. S., Dufresne, J.-L., Koshiro, T., Stevens, B., Wang, Z., and Yokohata, T. 2014. Origins of the solar radiation biases over the Southern Ocean in CFMIP2 models. *J. Climate*, **27**, 41–56.

Booth, J. F., Wang, S., and Polvani, L. M. 2013. Midlatitude storms in a moister world: lessons from idealized baroclinic life cycle experiments. *Climate Dyn.*, **41**, 787–802.

Butler, A. H., Thompson, D. W. J., and Heikes, R. 2010. The steady-state atmospheric circulation response to climate change-like thermal forcings in a simple general circulation model. *J. Climate*, **23**, 3274–3496.

Carlson, T. N. 1998. *Mid-Latitude Weather Systems*. American Meteorological Society, xx+507 pp.

Ceppi, P., and Hartmann, D. L. 2015. Connections between clouds, radiation, and midlatitude dynamics: A review. *Curr. Clim. Change Rep.*, **1**, 94–102.

Ceppi, P., and Hartmann, D. L. 2016. Clouds and the atmospheric circulation response to warming. *J. Climate*, **29**, 783–799.

Chang, E. K. M., Y., Guo, and X., Xia. 2012. CMIP5 multimodel ensemble projection of storm track change under global warming. *J. Geophys. Res. Atmos.*, **117**, D23118, doi:10.1029/2012JD018578.

Cotton, W. R., and Anthes, R. A. 1989. *Storm and Cloud Dynamics*. Academic Press, xii+880 pp.

Field, P. R., and Wood, R. 2007. Precipitation and cloud structure in midlatitude cyclones. *J. Climate*, **20**, 233–254.

Grise, K. M., and Medeiros, B. 2016. Understanding the varied influence of midlatitude jet position on clouds and cloud radiative effects in observations and global climate models. *J. Climate*, **29**, 9005–9025.

Hartmann, D. L. 2016. *Global Physical Climatology*. Second edn. Elsevier, 498 pp.

Holton, J. R., and Hakim, G. J. 2013. *An Introduction to Dynamic Meteorology*. Fifth edn. Academic Press, xvi+532 pp.

Hoskins, B. J., and Hodges, K. I. 2002. New perspectives on the Northern Hemisphere winter storm tracks. *J. Atmos. Sci.*, **59**, 1041–1061.

Lau, N.-C., and Crane, M. W. 1997. Comparing satellite and surface observations of cloud patterns in synoptic-scale circulation systems. *Mon. Wea. Rev.*, **125**, 3172–3189.

Li, Y., Thompson, D. W. J., and Bony, S. 2015. The influence of atmospheric cloud radiative effects on the large-scale atmospheric circulation. *J. Climate*, **28**, 7263–7278.

Lindzen, R. S., and Farrell, B. 1980. A simple approximate result for the maximum growth rate of baroclinic instabilities. *J. Atmos. Sci.*, **37**, 1648–1654.

Lorenz, D. J., and Hartmann, D. L. 2001. Eddy-zonal flow feedback in the Southern Hemisphere. *J. Atmos. Sci.*, **58**, 3312–3327.

Posselt, D. J., Stephens, G. L., and Miller, M. 2008. CloudSat: Adding a new dimension to a classical view of extratropical cyclones. *Bull. Amer. Meteor. Soc.*, **89**, 599–609.

Shaw, T. A., Baldwin, M., Barnes, E. A., Caballero, R., Garfinkel, C. I., Hwang, Y.-T., Li, C., O'Gorman, P. A., Rivière, G., Simpson, I. R., and Voigt, A. 2016. Storm track processes and the opposing influences of climate change. *Nat. Geosci.*, **9**, 656–664.

Trenberth, K. E., and Fasullo, J. T. 2010. Simulation of present-day and twenty-first century energy budgets of the Southern Ocean. *J. Climate*, **23**, 440–454.

Tselioudis, G., and Rossow, W. B. 2006. Climate feedback implied by observed radiation and precipitation changes with midlatitude storm strength and frequency. *Geophys. Res. Lett.*, **33**, L02704, doi:10.1029/2005GL024513.

Tselioudis, G., Zhang, Y., and Rossow, W. B. 2000. Cloud and radiation variations associated with northern midlatitude low and high sea level pressure regimes. *J. Climate*, **13**, 312–327.

Tselioudis, G., Lipat, B. R., Konsta, D., Grise, K. M., and Polvani, L. M. 2016. Midlatitude cloud shifts, their primary link to the Hadley cell, and their diverse radiative effects. *Geophys. Res. Lett.*, **43**, 4594–4601.

Vallis, G. K., Zurita-Gotor, P., Cairns, C., and Kidston, J. 2015. Response of the large-scale structure of the atmosphere to global warming. *Q. J. Royal Meteorol. Soc.*, **141**, 14791501.

INDEX